Atomic Force and Total Internal Reflection Fluorescence Microscopy for the Study of Force Transmission in Endothelial Cells

Anshu Bagga Mathur, George A. Truskey, and W. Monty Reichert
Center for Cellular and Biosurface Engineering, and Department of Biomedical Engineering, Duke University, Durham, North Carolina 27708-0281

ABSTRACT This paper describes the combined use of atomic force microscopy (AFM) and total internal reflection fluorescence microscopy (TIRFM) to examine the transmission of force from the apical cell membrane to the basal cell membrane. A Bioscope AFM was mounted on an inverted microscope, the stage of which was configured for TIRFM imaging of fluorescently labeled human umbilical vein endothelial cells (HUVECs). Variable-angle TIRFM experiments were conducted to calibrate the coupling angle with the depth of penetration of the evanescent wave. A measure of cellular mechanical properties was obtained by collecting a set of force curves over the entire apical cell surface. A linear regression fit of the force-indentation curves to an elastic model yields an elastic modulus of 7.22 $\pm$ 0.46 kPa over the nucleus, 2.97 $\pm$ 0.79 kPa over the cell body in proximity to the nucleus, and 1.27 $\pm$ 0.36 kPa on the cell body near the edge. Stress transmission was investigated by imaging the response of the basal surface to localized force application over the apical surface. The focal contacts changed in position and contact area when forces of 0.3–0.5 nN were applied. There was a significant increase in focal contact area when the force was removed ($p < 0.01$) from the nucleus as compared to the contact area before force application. There was no significant change in focal contact coverage area before and after force application over the edge. The results suggest that cells transfer localized stress from the apical to the basal surface globally, resulting in rearrangement of contacts on the basal surface.

INTRODUCTION

The cytoskeleton is an intricate three-dimensional network composed of actin filaments, intermediate filaments, and microtubules, where each component has a specific role in providing structure and function to an anchorage-dependent cell (Alberts et al., 1994; Maniotis et al., 1997; Yamada and Miyamoto, 1995). The cytoskeleton is considered the main stress-bearing component of the cell because of the restructuring of actin filaments, intermediate filaments, and microtubules upon exposure to force (Kim et al., 1989; Wechezak et al., 1989). The cytoskeletal components reorganize to offset the tension generated by the termination of cytoskeletal components at the adhesion sites (Davies, 1995; Ingber, 1997). Under stress conditions, actin filaments coalesce to form stress fibers that anchor at the focal contacts, which are the adhesion sites at the cell-substrate interface (Davies et al., 1993). Evidence suggests that f-actin is the main stress-bearing component of the cytoskeleton and is directly associated with the focal adhesions (Davies, 1995; Ingber, 1997; Davies et al., 1993). This study exploits the actin-focal adhesion connection to study the effect of mechanical forces on the dynamics of endothelial cell (EC) adhesion. In particular, the relationship between forces at the apical cell surface, such as the shear stress of flowing blood, and the distribution of focal contacts at the basal membrane are addressed.

One approach to examining the relationship between stress and the cytoskeleton involves observing changes in focal contacts after exposure to physiological shear stresses (Davies, 1995; Olivier et al., 1999). Previous flow studies of EC found that the stresses were nonuniformly distributed over the apical cell surface during shear flow, making it difficult to interpret the subsequent flow-induced changes in focal contacts (Olivier et al., 1999). Flow studies unfortunately provide limited information about cell mechanics. Initial studies with micropipette aspiration concentrated on red blood cells and granulocytes mechanics modeled to calculate the viscous and elastic properties (Evans, 1989; Evans and Yeung, 1989). The cell membrane was modeled to be elastic, enclosing a viscous fluid of the cytoplasm. Cell membrane mechanics was also examined by membrane tether extraction (Hochmuth et al., 1996), pico-force transducer (Evans et al., 1995; Simson et al., 1998), and laser optical trap techniques (Svoboda et al., 1992; Bronkhorst et al., 1995; Sheetz and Dai, 1996). Other than the shear flow studies, the micropipette-based techniques were limited to providing mechanical properties of detached cells. The technique of magnetic bead microrheometry (Bausch et al., 1998) has proved to be a useful measure of local viscoelastic properties of anchorage-dependent cells. However, studying detached anchorage-dependent cells can result in elastic and viscous properties that differ for adherent cells. For adherent cells, Wang and Ingber (Wang et al., 1993; Wang and Ingber, 1994; Wang and Ingber, 1995) manipulated the cell cytoskeleton with magnetic beads to study links between applied twisting stress, stiffness, cell surface

Received for publication 13 September 1999 and in final form 4 January 2000.

Address reprint requests to Dr. W. Monty Reichert, Department of Biomedical Engineering, Box 90281, 136 Hudson Hall, Duke University, Durham, NC 27708-0281. Tel.: 919-660-5151; Fax: 919-660-5362; E-mail: reichert@acpub.duke.edu.

0006-3495/00/04/1725/11 $2.00

adhesion molecules, and the cytoskeleton. They found that as the applied twisting stress on the integrins was increased, there was a more than threefold increase in membrane stiffness. Although Wang and Ingber provided insight into the link between twisting force and the cytoskeleton, the effect of normal forces on the cell apical surface was not examined because of the design of the instrument. In addition, the magnetic twisting technique cannot directly assess a relation between applied forces and focal contact dynamics. Thus there is a need to more precisely determine the correlation between mechanical properties and the effect of apically applied forces on anchored cells, specifically with respect to force-induced changes in the cytoskeletal components, such as the focal contacts.

Atomic force microscopy (AFM) is a facile tool for imaging, force application, and molecular interaction measurements. A recent study combined AFM with reflection interference contrast microscopy to study protein-ligand interactions (Stuart and Hlady, 1999). The topography of the apical cell membrane and the underlying cytoskeleton of live cells anchored to substrates can be easily imaged by AFM. AFM also allows the precise application of calibrated deformation to the cell at nanometer resolution (Weisenhorn et al., 1993; Radmacher et al., 1996; Hofmann et al., 1997; Rotsch et al., 1997, 1999; Braet et al., 1998; Ricci et al., 1997; A-Hassan et al., 1998; Chang et al., 1993). The elastic modulus of cells was determined by deforming the apical surface of the cell and fitting the deformation curve to the Hertz model that predicts the elastic response of the cell (Radmacher et al., 1996; Hofmann et al., 1997; Rotsch et al., 1997, 1999; Braet et al., 1999; Ricci et al., 1997; A-Hassan et al., 1998; Chang et al., 1993). Using the Hertz model, the elastic modulus of different cells was found to range from 1 to 200 kPa, depending on the cell type and the location on the cell apical surface (Radmacher et al., 1996; Hofmann et al., 1997; Rotsch et al., 1997, 1999; Braet et al., 1999; Ricci et al., 1997). In a more recent study, leading and stable edges of mobile fibroblasts were compared for stiffness by use of the AFM (Rotsch et al., 1999). They reported the leading edge to be softer than the stable edge (3–5 kPa versus 12 kPa). An elastic modulus of 2 kPa was also reported for liver endothelial cells (Braet et al., 1999). It is interesting to note that their recent studies (Rotsch et al., 1999; Braet et al., 1999) have resulted in lower elastic modulus values over the cell as compared to their earlier studies (Radmacher et al., 1996; Hofmann et al., 1997; Rotsch et al., 1997), which may be a result of a different cell type or a change in experimental conditions, for example, scan rate and loading forces. The mechanical response of epithelial cells was analyzed by calculating an apparent spring constant of 0.002 N/m for the apical cell surface of the cell (Schoenenberger and Hoh, 1994). Long-term AFM imaging forces were found to disrupt the cytoskeletal components and lower the overall elastic modulus of the cell (Chang et al., 1993). These studies show that AFM is well suited for determining the mechanical properties as well as simultaneously perturbing the cell membrane.

Various cell perturbations, such as shear stress (Olivier et al., 1999; Davies et al., 1993), AFM (Henderson and Sakaguchi, 1993), and glass needle (Heidmann et al., 1999), have been combined successfully with optical microscopy to study the cytoskeleton. AFM was combined with an optical microscope to image the cytoskeleton (Henderson and Sakaguchi, 1993), but this study did not examine cell perturbation simultaneously, because the cells were fixed. AFM was also used for topographic mapping of an endothelial cell layer subjected to shear stress (Barbee et al., 1994). Shear stress studies were conducted with total internal reflection fluorescence microscopy (TIRFM), an interfacial optical technique, to follow focal adhesion movement under shear flow conditions (Olivier et al., 1999). More recently, green fluorescent protein (GFP)-labeled actin and microtubule dynamics were studied by indenting and extending the cell membrane with a glass needle and observing changes via fluorescence microscopy (Heidmann et al., 1999). Their results showed that the glass needle deformations produced a local response rather than a global response of the actin filaments. The mechanical instruments, combined with an optical microscope, although useful, do not provide information on the relationship between stress and the focal adhesion element of the cytoskeleton.

In this paper we describe a combination of AFM and waveguide TIRFM designed to provide simultaneous mechanical force transmission measurements and focal contact dynamics in cultured cell monolayers (Fig. 1). TIRFM excites fluorescence in the basal membrane of cells attached to the waveguide surface, while an AFM tip introduced from above the coverslip probes the apical membrane of the same cells. Simultaneous application of AFM and TIRFM data allows one to track the effect of localized force application at the apical membrane on the cell's focal contact size and position at the basal membrane.

MATERIALS AND METHODS

Cell culture and staining the cell membrane

Human umbilical vein endothelial cells (HUVECs) (Clonetics, Walkersville, MD) were grown in gelatin-coated T25 flasks in 5% CO_2 at 37°C in Endothelial Basal Medium (EBM) (Clonetics) supplemented with EGM singlequot growth factors (Clonetics) until confluent. Passages 1–4 were used for these experiments. Flasks containing cells were trypsinized and then centrifuged to form a pellet. The cell pellet was dispersed and incubated with 5 mg/ml of Dil C_{18} (Molecular Probes, Eugene, OR) in a 300 mM sucrose solution for 10 min. The cells were subsequently cultured in the supplemented EBM on gelatin-coated glass coverslips for 24 h. After 24 h, 2% (v/v) HEPES buffer in supplemented EBM was added to the cells and incubated for 1 h.

Rhodamine-phalloidin staining

HUVEC cultured for 24 h were immersed in Histoprep Buffered 10% Formalin (Fisher Scientific, Pittsburgh, PA) to fix the cells. After 10 min,

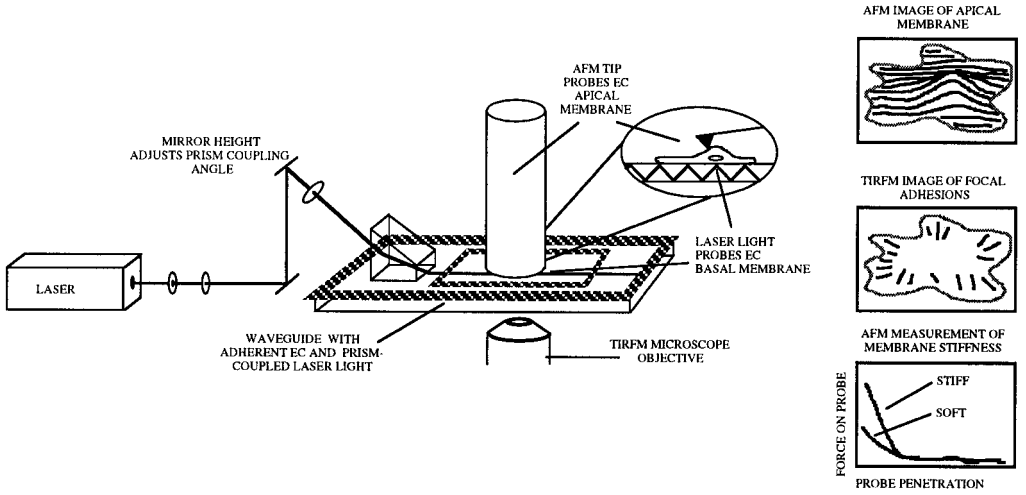

FIGURE 1 AFM-TIRFM simultaneously images the apical and basal surfaces of an endothelial cell. An Ar^+ ion laser beam ($\lambda = 488$ nm) was totally internally reflected via a glass prism at selected angles above the critical interfacial angle. The beam illuminated the cell-substrate contacts while the AFM cantilever perturbed the cell.

formalin was aspirated and 5 ml of acetone was added at −20°C for 3 min. Permeabilized cells were washed with phosphate-buffered saline, and 0.6 μg/ml of rhodamine-phalloidin (Sigma Chemicals, St. Louis, MO) in phosphate-buffered saline was added to the slide to label actin filaments. The cells were subsequently imaged using TIRFM and confocal microscopy.

TIRFM imaging

Figs. 1 and 2 schematically illustrate the AFM/TIRFM apparatus. A 4.1 × 4.7 cm anodized aluminum plate milled with a 3.8 × 1.8 cm opening and 0.1-cm thickness was sealed to the cell-plated coverslip surface by a layer of silicon lubricant (Dow Corning Corp., Midland, MI) and then secured to the 12.3 × 7.2 cm fluid cell with screws. This produced a 0.2-cm-deep liquid reservoir into which growth medium containing HEPES buffer was added to maintain cell viability. The medium was changed periodically to control the temperature and the pH fluctuations. The end of the slide was cleaned with lens paper immersed in 70% ethanol to remove growth media and cell debris from the surface. A small drop of coupling oil (mineral oil, $n = 1.515$; Cargille Labs, Cedar Grove, NJ) was placed on one end of the coverslip to accommodate the coupling prism (BK-7 glass, $n = 1.51$; Karl Lambretch Corp., Chicago, IL). The entire assembly was fixed to the stage of the AFM/TIRFM apparatus as described below.

The assembled fluid cell was secured to the stage of an inverted microscope (Zeiss Axiovert 100 TV inverted microscope; Carl Zeiss, Thornwood, NY) with a specially designed mount and stage that accommodates an AFM tip. The reservoir opening accommodates the AFM tip as described below. A focused beam of laser light ($\lambda = 488$ nm; 2.3 kW; Ion Laser Technology; model 5450ASL-00C, type F148/B091) is coupled to the coverslip via the prism, propagating as a streak under the silicone sealant and beneath the cells in the liquid reservoir. Raising and lowering the final reflecting mirror varies the prism coupling angle and thus the propagation angle (θ_i) of the light inside the coverslip. This allowed us to vary the evanescent wave intensity that illuminates the underside of the cells plated to the coverslip surface. This optical configuration is a slight modification of the one reported previously (Axelrod et al., 1984). The inverted microscope was equipped with a ST-6 CCD camera (Santa Barbara Instruments Group (SBIG), Santa Barbara, CA). A long-pass inter-

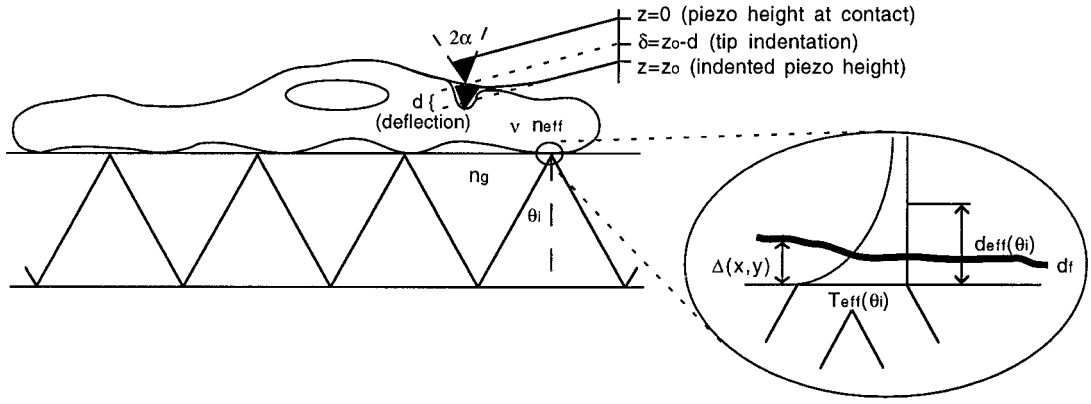

FIGURE 2 A schematic illustration of an evanescent wave illuminating the basal membrane and an AFM probe interacting with the apical membrane of an attached cell. An evanescent wave is created at the glass-cell interface, which selectively illuminates the focal contacts on the basal surface as the AFM probe deforms the membrane from above. Note that this figure is not drawn to scale. The AFM probe does not entirely penetrate the membrane.

ference filter (520 nm, LP 520; Chroma Technology Corp., Brattleboro, VT) was placed between the objective and the camera to remove the excitation wavelength and pass the emission wavelength. The camera was connected to a Macintosh G3 installed with CCDOPS software (SBIG) to grab fluorescent images. The image exposure time ran from 1 to 3 s, depending on the intensity of the TIRFM image.

Modeling of TIRFM images

Fig. 2 includes a schematic illustration of an evanescent wave illuminating the basal membrane of an attached cell. The theory of TIRFM (Reichert and Truskey, 1990) and its application to the study of cell adhesion (Burmeister et al., 1994, 1998) was described in detail elsewhere. Briefly, a beam of light incident from glass to the glass/water interface will undergo total internal reflection (TIR) if the incident angle (θ_i) with respect to the interfacial normal exceeds the critical angle (θ_c); i.e., $\theta_i > \theta_c$, where $\theta_c = \sin^{-1}(n_w/n_g)$, and n_g and n_w are the glass and water refractive indices, respectively. The evanescent wave penetrates with exponentially decaying intensity just a few tenths of a micron into the interface and excites fluorescence confined to the interfacial region. In the case of TIRFM of cells, the cell membrane is so thin (4 nm) compared to the wavelength of the incident light that the intensity of transmitted light across the membrane is essentially constant (Burmeister et al., 1998). Thus the following approximate expression describes the distance-dependent TIRFM image intensity of an anchorage-dependent cell with a fluorophore-labeled cell membrane:

$$F(x, y, \theta_i) = KT_{eff}(\theta_i)\exp[-\Delta(x, y)/d_{eff}(\theta_i)] \quad (1)$$

where K is an experimental constant, $T_{eff}(\theta_i)$ and $d_{eff}(\theta_i)$ are the effective Fresnel transmission coefficient and depth of penetration of the evanescent wave, respectively, and $\Delta(x, y)$ is the separation distance between the membrane and the substrate. T_{eff} and d_{eff} are functions of the effective refractive index n_{eff} of the anchored cell ($n_{eff} = n_g\sin(\theta_c)$), the incidence angle θ_i, and the wavelength of light λ. In a given experiment, θ_i and n_{eff}/n_g were considered fixed, making $T_{eff}(\theta_i)$ and $d_{eff}(\theta_i)$ constants. The cell-substrate separation distance $\Delta(x, y)$ was obtained from the slope of the natural log of the image intensity plotted against the inverse of the d_{eff}, i.e., a plot of $\ln[F(x, y, \theta_i)/\cos^2\theta_i]$ versus $1/d_{eff}(\theta_i)$. Point-by-point application of the above relationship via digitized imaging allows one to transform TIRFM data directly into spatial maps of membrane/substrate separation distances (Burmeister et al., 1994, 1998).

The analysis of TIRFM images was limited by the effective refractive index of the cell and the critical angle above which the light totally internally reflects (Burmeister et al., 1998). The critical angles for the glass-cell membrane interface have been shown to vary from 63° to 66° for effective refractive indices of 1.358–1.374, because focal contacts are dynamic entities. Other parameters influencing the quality of the TIRFM images are background interference, scatter from the fluorescing contacts, photobleaching, and dye aggregation or exclusion (Burmeister et al., 1998).

AFM imaging

A Bioscope AFM (Digital Instruments, Santa Barbara, CA) probe was mounted on the inverted microscope once the waveguide coupling was complete. Contact-mode AFM imaging under fluid was conducted using 200-μm oxide-sharpened silicon nitride cantilevers (Digital Instruments) with spring constants of 0.03–0.05 N/m and a cone angle of 35°. A thermal vibration-based program, installed in the Nanoscope 4.23 r3 version, was used to calculate the spring constant (N/m) for a specific cantilever type. The cantilever was calibrated before each experiment.

The calibrated cantilever was placed on the fluid holder and connected to the Bioscope before the AFM/TIRFM experiment was begun. A drop of growth medium was added to the cantilever holder before the entire scanner was inverted on top of the glass coverslip. The stepper motor was used to move the piezo closer to the sample until the cantilever was visualized through the microscope above the cells. To begin scanning, the scan size was set to 0 nm and the scan rate to 0.1 Hz. This was done to minimize tip-cell contact until the contact force was reduced using the setpoint. The setpoint was decreased until the tip came off the surface and then increased by one increment to restore contact. Imaging was conducted by increasing the xy scan size incrementally until the entire cell was visible. The xy scan rates used for imaging range from 0.1 to 0.5 Hz for a scan size as large as 80 μm.

Force measurements

Force curves were obtained in the force calibration mode. The z-scan velocity ranged from 0.5 to 1 μm/s. The AFM-TIRFM experiments were conducted on the HUVECs by applying a force of 0.3–0.5 nN to the cell in the force calibration mode and simultaneously imaging the changes in focal contacts. A constant force was applied for 1 min on the apical cell surface, and focal contact images were taken before and after the force application. After the force was removed, the cell was allowed to relax, and images were taken at 1-min intervals for 5 min.

Modeling of AFM probe cell indentation

Fig. 2 also contains a schematic illustration of an AFM tip interacting with the apical cell surface of an attached cell (Radmacher, 1997). The cell deformation was characterized by applying the Hertz model that describes the indentation of a homogeneous/semiinfinite elastic material by a stiff material with a defined geometry (Weisenhorn et al., 1993; Radmacher et al., 1996). The indenting material, the AFM tip, was defined to be conical in shape. Defining the tip geometry was important because the contact area between the tip and the sample increased as the indentation depth increased. The Hertz model defined the elastic response of the cell to a deformation as follows (Weisenhorn et al., 1993; Radmacher et al., 1996; Radmacher, 1997):

$$F = \delta^2[2E\tan(\alpha)/\pi(1-\nu^2)] = kd \quad (2)$$

$$\delta = z - d \quad (3)$$

$$(z-d)^2[2E\tan(\alpha)/\pi(1-\nu^2)] = kd \quad (4)$$

where F is the applied force calculated by kd, z is the piezo height, and d is the cantilever deflection The difference between z and d is the indentation δ. The cell elastic modulus, E, and Poisson's ratio, ν, define the material properties. The Poisson's ratio was assumed to be 0.5 because the cell was considered incompressible. The cantilever properties were defined by the opening angle α and the cantilever spring constant k. The average elastic modulus values were reported for over the nucleus, over the cell body near the nucleus, and the cell body near the edge of the cell. All data are given as mean ± SEM.

RESULTS

Verification of TIRFM imaging

Fig. 3 contains the angularly dependent individual focal contact intensities used to confirm that TIRFM images were collected from the cells at the coverslip surface. An application of Eqs. 1–4 via digitized imaging allowed the transformation of focal adhesion intensities directly into membrane/substrate separation distances. TIRFM images were collected from HUVECs as the propagation angle (θ_i) of the

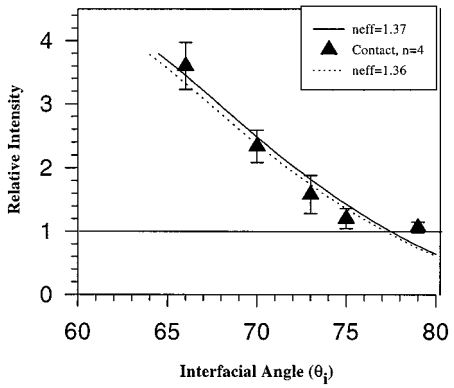

FIGURE 3 A plot of variation in focal contact intensity with interfacial angle. The data fit the predicted curve for the refractive index (n_{eff}) of 1.36–1.37, for the three-layer VA-TIRFM model that models the penetration of the evanescent wave into the glass-cell interface. The horizontal line represents the background value.

incoupled laser light was varied from 66° to 80° for 488-nm light, because both the apical and basal surfaces were illuminated below the critical angle for this system (64°) (Burmeister et al., 1998). The TIRFM intensities tend to disappear into the noise of the system (horizontal line) at higher angles.

Individual focal adhesion intensities of four cells (three focal adhesions per cell) were averaged and plotted as a function of angle. Focal adhesions were identified by thresholding at distances up to 50 nm from the surface. The decrease in propagation angle from 66° to 80° caused the evanescent depth of penetration (d_{eff}) to vary from 145 to 59 nm and the transmission coefficient (T_{eff}) to drop from 3.37 to 0.62. As predicted, the intensity of the individual focal contacts measured by TIRFM decreased with increasing propagation angle. The experimental data were fit to the simplified three-layer TIRFM model developed for the variation of evanescent intensity (T_{eff}) at a glass-cell interface for an anchorage dependent cell, where n_{eff} was 1.37 and 1.36 (Burmeister et al., 1998). A nominal separation distance of 31 $\pm$ 19 nm was calculated from the slope of linear regression fit of $\ln[F(x, y, \theta_i)/\cos^2\theta_i]$ versus $1/d_{eff}(\theta_i)$. The reported separation distance accounts for both focal contact ($<$15 nm) and close contacts ($<$50 nm) (Burmeister et al., 1998). Subsequent experiments with the AFM/TIRFM were conducted at an interfacial angle of 71° because the background interference and contribution from the dorsal membrane were negligible at this angle. The depth of penetration at 71° was calculated to be 85 nm for 488-nm light.

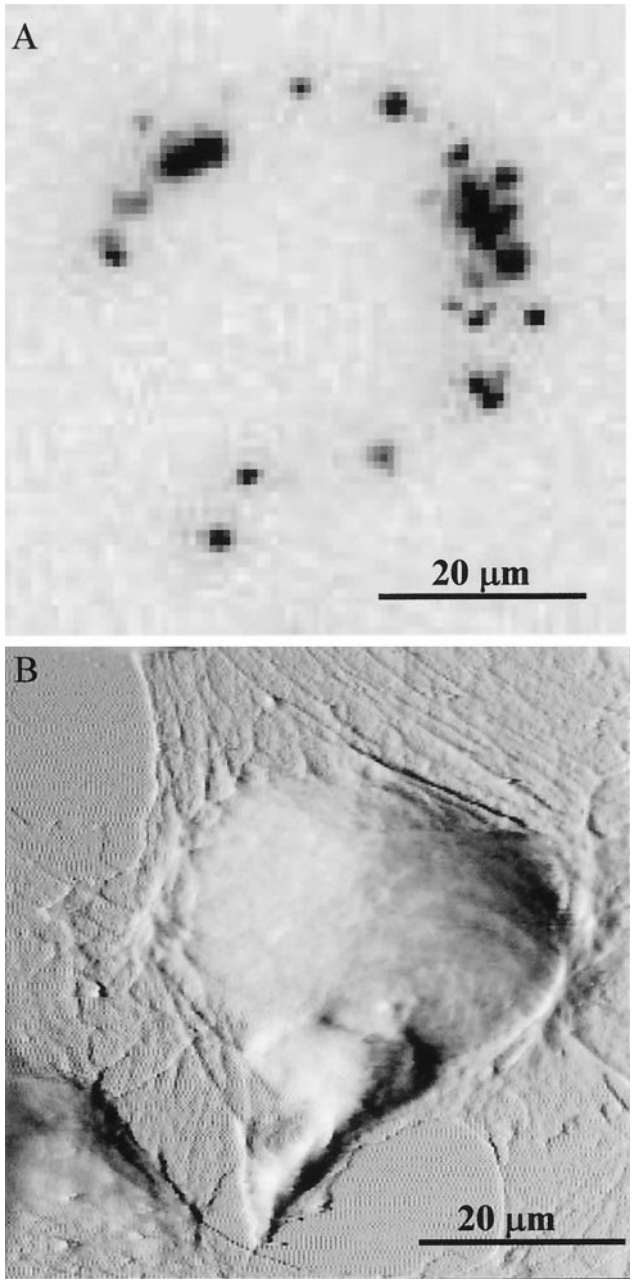

FIGURE 4 TIRFM image of fluorescently labeled cell membrane showing the focal contacts of the basal cell membrane (*A*) and a topography of the apical cell membrane (*B*) showing the cytoskeleton of a live human umbilical vein endothelial cell (HUVEC) imaged by simultaneous TIRFM and AFM. The black regions in *A* represent the cell-substrate contacts. The darker the region the closer it is to the glass-cell interface; the lightest region is 85 nm from the glass. The cell was cultured on a collagen-coated glass surface for 24 h.

Simultaneous AFM AND TIRFM imaging

Fig. 4 shows the basal and apical membranes of a single live DiI-stained endothelial cell imaged simultaneously by TIRFM and AFM. Fig. 4 *A* shows the TIRFM image of the basal membrane threshold at 85 nm. The darker regions correspond to the focal adhesion sites, where the darkest shading corresponds to the regions of the basal membrane closest to the substrate. After 24 h of adhesion to the glass substrate, the focal adhesion sites were more prominent at the periphery of the cell and minimally present beneath the

nucleus. Fig. 4 *B* is the corresponding AFM image of the apical cell membrane collected in deflection mode to show the cytoskeleton of the cell.

The nucleus was raised away from the substrate and was the highest point, 3.5 μm, as measured by the AFM. AFM also allows the nanoscale imaging of the cytoskeletal stress fibers, which are prominent throughout the apical surface of the cell and protrude from the main cell body to attach the cell to the substrate.

Determination of cell elastic modulus

Force-indentation curves for regions of an endothelial cell apical surface over the nucleus and over the cell body are shown in Fig. 5 *A*. The force was calculated from the spring constant and the deflection of the cantilever ($f = kd$). The indentation was determined from the difference in the z movement of the piezo and the deflection of the cantilever (Radmacher et al., 1996). For z values less than zero (not shown), the piezo was not yet in contact with the cell and the force was zero. The cantilever tip comes in contact with the cell at $z = 0$, and the force increases with indentation beyond this point. The same indentation curve was obtained for an apical region over the cell body. The indentation depth needed to produce the same cantilever deflection was much larger on the cell body than on the nucleus for comparable forces, indicating that the cell body was more deformable. The apparent spring constant over the cell body was calculated to be 0.0004 N/m, fourfold lower than the value of 0.016 N/m calculated over the nucleus.

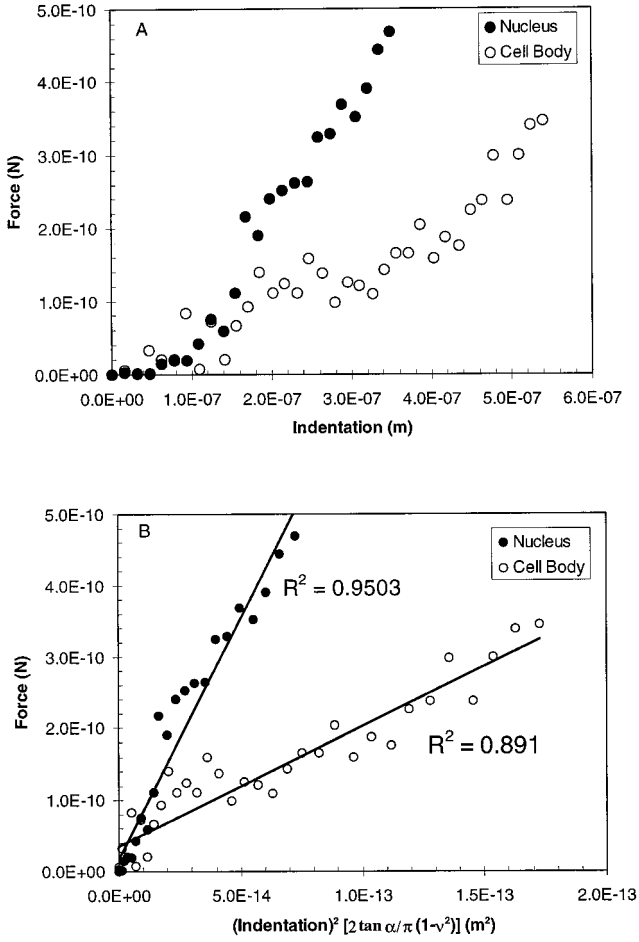

FIGURE 5 A set of force-versus-indentation curves (*A*) for the deformation of the apical surface of a HUVEC by an AFM probe collected over the nucleus and the cell body. A linear regression fit to the Hertz model was used to calculate the elastic modulus of the cell in the two regions in *B*.

Fig. 5 *B* shows the Hertz transformation of the force-indentation data found in Fig. 5 *A*. A linear regression fit of the data to the Hertz model corresponding to larger deflections yields an apparent elastic modulus of 7.22 $\pm$ 0.46 kPa ($n = 6$) over the nucleus and 1.27 $\pm$ 0.36 ($n = 6$) on the cell body near the edge. Intermediate values of 2.97 $\pm$ 0.79 kPa ($n = 6$) were obtained by moving away from the nucleus toward the edge of the cell. It is not clear from the data over the cell body that the material is behaving in a purely elastic manner, because the linear regression fit of the Hertz model gives R^2 values of less than 1. The deviation from the Hertz model may be attributed to viscous contributions, heterogeneity in the cell, and/or tip geometry. Thus other models will be examined before a true elastic modulus of the cell is calculated (Christensen, 1971).

Stress transmission

Results of the force application study indicated that significant changes occurred in cell-substrate contacts in position and focal contact distribution when localized forces in the 0.3–0.5-nN range were removed. Fig. 6 *A* shows the distribution of the focal contacts before a force of 0.35 nN was applied near the nucleus (indicated by *). The background is indicated by yellow, and the focal adhesions appear as blue-black regions around the periphery of the cell. The darker the focal contact, the closer it is to the glass substrate. The force was applied for 1 min and was removed before the cell was allowed to relax for 5 min. Fig. 6 *B* shows the arrangement of focal contacts after 5 min of relaxation after force application. The subtraction of Fig. 6 *A* and Fig. 6 *B* is shown in Fig. 6 *C*. The background and no change in the location of the contacts are shown by the color red. The yellow regions represent an increase in focal adhesions, while the blue-black regions show a decrease in focal adhesions. A qualitative assessment of the images suggests that there are global focal contact rearrangements due to the applied force. While the small contacts in close lateral proximity moved toward each other, the larger contacts moved away from each other. A time-lapsed TIRFM "video" of the cell in Fig. 6 is available on the web at http://www.duke.edu/~abm4/tirf-afm.html.

Fig. 6 *D* shows the initial arrangement of focal contacts before a force of 0.3 nN was applied for 1 min on the edge

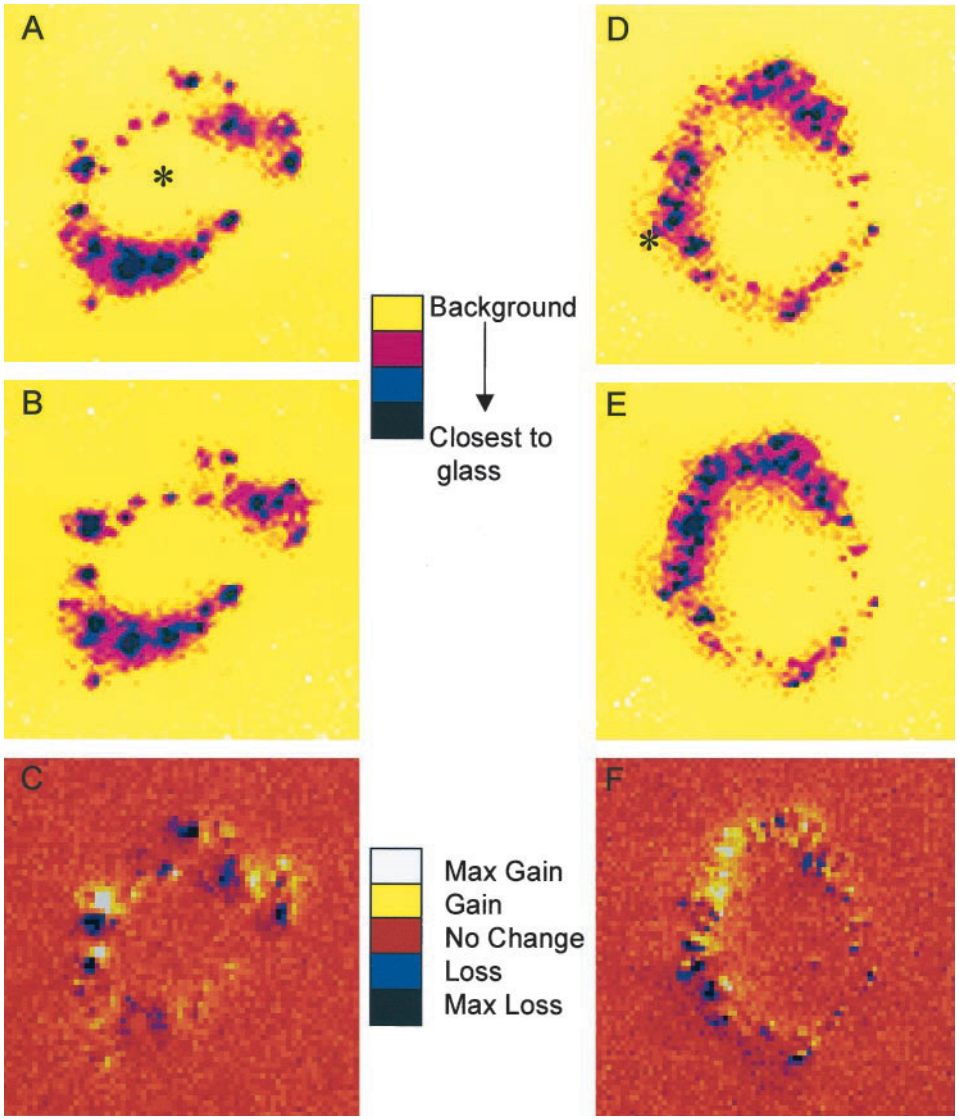

FIGURE 6 The distribution of the focal contacts before 0.35 nN force was applied near the nucleus (indicated by *) is shown in *A*. The background is shown by yellow, and the focal adhesions appear as blue-black regions around the periphery of the cell. After force was applied for 1 min and removed, the cell was allowed to relax for 5 min. The arrangement of focal contacts after 5 min is shown in *B*. The subtraction of *A* and *B* is shown in *C*. The background and no change in the location of the contacts are shown by the color red. The increase in focal contacts is shown in yellow and loss is shown in blue. The initial arrangement of focal contacts before a 0.3 nN of force was applied to the edge is shown in *D*. The force was applied on the outer periphery (marked by *), and the focal contacts relocated after 5 min of relaxation are shown in E. The subtraction of images *D* and *E* is shown by a region with an increase in focal contacts in yellow and the decrease in blue-black (*F*).

(marked by *) and then removed before the cell was allowed to relax for 5 min. The force was applied on the outer periphery where focal adhesions were primarily present. Fig. 6 *E* shows the position of focal contacts after 5 min of relaxation, and Fig. 6 *F* shows the subtraction of images taken before and 5 min after force application. There is a global movement of focal adhesions during the 5-min relaxation period, as evident from the loss of focal contacts on the outer edge of the cell and then the gain on the inner side. A systematic increase in focal contacts in the region of preexisting contacts occurs over a 5-min period.

The response of a cell to a force on the edge of the cell was variable and appeared to be dependent upon the shape of the cell and location of the applied force. The increase or decrease in focal contact area depended upon whether the cell was slightly elongated or had a rounded appearance. The response was also dependent on whether the location of the applied force was near preexisting contacts, clusters or sparsely populated contacts, the tail end of the cell, or the side edge. In some cases, there was a global loss of focal contacts while the cell was moving, while in other cases one end was moving more rapidly than the other, because the more stagnant end was increasing in focal contact area.

A common observation for force applied over either the nucleus or the edge was the coordinated movement of neighboring large focal contacts. The neighboring large focal adhesions increased in size to become larger only until they contacted each other, at which point there was either an increase of one focal contact and a decrease of the other, or both separated and appeared to decrease in size (Fig. 6, *A–C*).

Fig. 7 shows population data for the variation in focal contact coverage area over a 5-min period after the removal of the force. Cell surface indentation over the nucleus yielded an initial increase ($p < 0.05$) in the focal contact coverage area after removal of the applied force. Unlike the

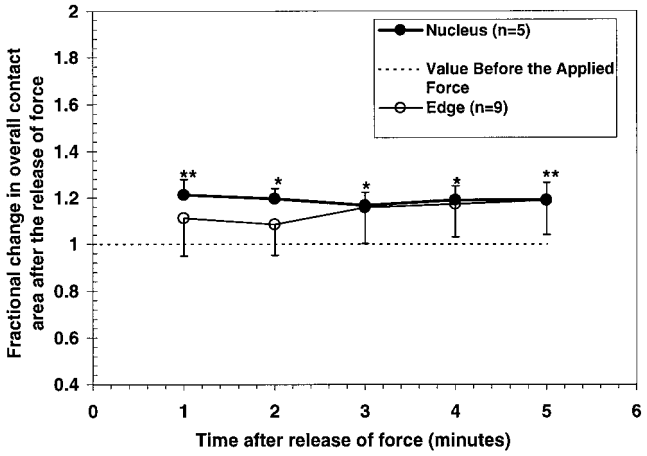

FIGURE 7 A graph of change in the focal contact area for the 5 min of relaxation of cells after a force of 0.3–0.5 nN was released over the nucleus and the edge of the cell. There was a significant increase in the focal contact coverage area as compared to the initial value before force application and after the force was removed over the nucleus. Although all time points differ from the initial value, there was not a significant difference within the 5-min time intervals as the focal contacts were reorganizing. $^{**}p < 0.01$; $^{*}p < 0.05$. There was no significant change in average focal contact coverage area after the force was released over the edge of the cell.

nuclear region, the average response of the cells to indentation over the cell edge was not significantly different. However, there were clear qualitative differences between before and after images.

DISCUSSION

This paper describes the integration of AFM and TIRFM to observe the transmission of force between mechanical perturbations of the apical cell surface and focal contact dynamics at the basal cell membrane. Perhaps the most surprising observation was that the precise localized mechanical perturbations in any region induced by the AFM tip resulted in a global rearrangement of focal contacts at the basal membrane. Furthermore, the system was used to characterize the stiffness of the apical cell surface. The apical cell surface displayed elastic moduli of 1.27–2.97 kPa over the cell body and an average of 7.22 kPa over the cell nucleus. Although the response remained global whether the region was soft or stiff, force application over the nuclear region appeared to produce a more consistent change in contact area, while the contact area responded variably to the force on the edge of the cell.

In both instances, the mechanical response of cells varies because of the complex nature of the cytoplasm that contains water, organelles, and the cytoskeletal components organized to offset the stress experienced at the apical surface. However, in view of previous reports and what is known about cytoskeletal structure, we can draw several inferences from this work. The localized force leads to a global change in the focal adhesions observed by the movement of the focal adhesions and the changes in focal contact coverage area (Figs. 6 and 7). The fact that the effect of local perturbation is global shows that the cytoskeleton may be responsible for integrating the response. Because the actin filaments span the entire cell and are contractile in nature, they provide the flexibility needed to respond globally to a localized force.

Over the nucleus, the initial rise ($p < 0.05$) in focal contact area indicated a response to the applied force, but no relaxation of focal contacts to their original values was evident within the first 5 min. The viscous relaxation of the cell or formation of stable contacts might affect these results. The viscoelastic modeling of micropipette deformation of detached bovine aortic endothelial cells resulted in a relaxation time of 2.5 min (Sato et al., 1990). The relaxation time may be higher in the current study because the cells were anchored and the perturbation was highly localized as compared to the results of Sato et al. Moreover, the physical relaxation of the apical surface may not correspond linearly with the chemical bond relaxation at the focal adhesions. Because the contact areas did not significantly decrease over the 5-min period (for the nuclear region), the cell acquired a new configuration, as indicated by the increased contact area.

Within 1 min of the removal of the force on the edge, the focal contacts appear to move globally away from the location of the applied force. The movement was usually associated with a loss in focal contact coverage area initially. For the large cell body to move, the existing contacts would have to be dissociated from their original position and associate again at a downstream location. There was also a tendency of preexisting contacts to increase in coverage area either individually, by coalescing with other contacts, or by the formation of new contacts in the region of preexisting contacts. The collaborative response of larger focal contacts in close proximity may be a stress-bearing mechanism. Each of these events must result from the transient aspect of the available integrin-dependent ligands at the cell-substrate interface.

In assessing the individual behavior of edge-perturbed cells during the 5-min relaxation period, it was evident that the response may depend on critical focal contact coverage area and the distribution of focal contacts present near the location of the applied force. The various responses observed were 1) only global movement of focal contacts; 2) movement on one end and an increase in focal contact area on the other end, which has a critical population and coverage area of contacts; and (3) an increase in focal contact area only, with minimal contractual movement.

Previous studies revealed that nonuniform distribution of stresses over the entire apical region causes a global change in focal contacts (Olivier et al., 1999; Davies et al., 1993). On the other hand our data indicate that local stresses also cause a global motion of focal contacts. Previous shear flow

studies on the endothelium also indicated that there was convergence of focal adhesions minutes after the onset of flow. This finding was in accordance with our results that there was a movement of small contacts toward each other when localized force was applied (Davies et al., 1993).

The average elastic modulus values over the cell body of the anchored HUVEC, determined in this study with the AFM (1.27–2.97 kPa), were similar to the values obtained by micropipette suction and recent AFM measurements. Elastic moduli previously reported on detached EC range from 0.3 to 3 kPa for nonoriented and oriented bovine aortic EC (Theret et al., 1988), which was measured using micropipette suction and an analytical model. A recent AFM study reported the elastic modulus for the leading edge of mobile fibroblasts to be 3–5 kPa (Rotsch et al., 1999) for lower loading forces of 80–320 pN. Furthermore, AFM measurement on liver endothelial cells yielded an elastic modulus of 2 kPa (Breat et al., 1998).

The observation that the apical cell surface of EC was stiffer over the nucleus (7.22 kPa) as compared to the remaining cell body (1.27–2.97 kPa) differs from the finding (Radmacher et al., 1996) that elastic modulus values over the nucleus of platelets were lower (1.5–4 kPa) than the anchoring edges of platelets (100 kPa). Although platelets may be inherently stiffer than the EC, the peripheral regions of the platelets are thin and close to the anchoring substrate. Factors such as higher scan rates, indentation depths, and loading forces could cause the indenting cantilever to sense the stiff substrate, resulting in the higher elastic modulus values observed by Radmacher et al. (1996). In the current study, the scan rates and loading forces were chosen to minimize viscous effects as judged by the absence of hysteresis in the extension-retraction curves. Consequently, the elasticity values obtained in this study were smaller than previously reported by other authors using the AFM.

The elastic modulus values reported here were determined using a purely elastic model (the Hertz model) for a semiinfinite material. Although the data fit the Hertz model in most regions over the cell with an R^2 greater than 0.8, there was a noteworthy deviation from the linear fit in the initial portion of the curve. The deviation points to the fact

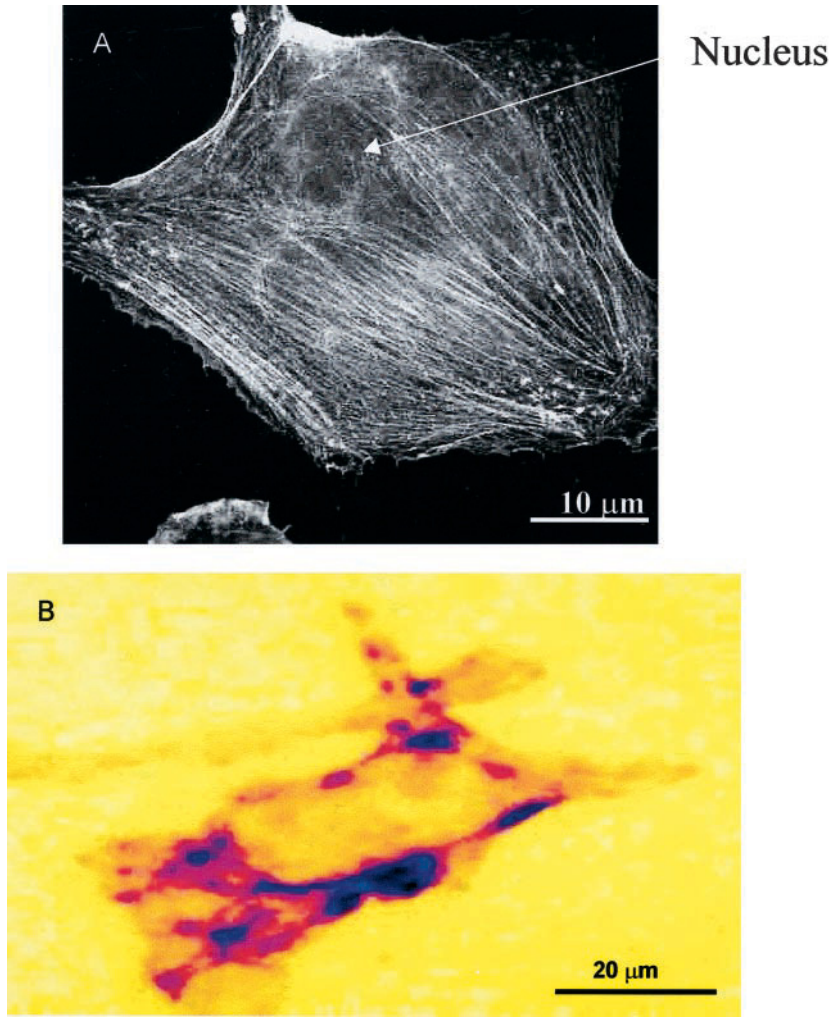

FIGURE 8 Confocal (*A*) and TIRF (*B*) microscopy images of rhodamine-phalloidin-stained HUVEC, showing the actin filaments stretching across the cell. The filaments are going around the circular region in the middle (marked as the nucleus by an *arrow*) (*A*) and terminate at the focal adhesions (shown as *blue-black regions around the periphery in B*).

that the cell is not purely elastic. Viscous effects may play a role at higher scan rates (Radmacher et al., 1996), although this may not be the primary factor in this case. Because the viscous effects were minimized (low scan rates), the cell deformation was modeled as purely elastic, semiinfinite material as a reasonable approximation. The cell response to the indentation could be elastic, but the deformation behavior may be complex because the cell is a live entity and may be adapting and responding to the indentation, resulting in a heterogeneous deformation.

Although a limitation of this study was not showing the direct contribution of the cytoskeleton in force transmission, the relationship between local stress and global response has been established. Future work using the AFM-TIRFM device will be conducted with green fluorescent protein (GFP)-labeled cytoskeletal components such as actin and vinculin. Nevertheless, this study indicates that the cell can integrate a localized stress into a global response. This mode of transmission could have occurred through the actin filaments that encompass the nucleus and span the cell, as shown in Fig. 8 *A*, a confocal image of the rhodamine-phalloidin-stained actin filaments of a HUVEC. Fig. 8 *B* is a TIRFM image of different HUVECs stained with rhodamine-phalloidin imaged to show the termination of the actin filaments at the focal contacts. Because the evanescent wave illuminates only 85 nm above the glass surface, the actin filaments terminating in the focal adhesions were illuminated. Taking both images into account, it is apparent that actin filaments infiltrating the cell, skirting around the nucleus, and terminating at the focal contacts could result in global motion of the focal contacts.

CONCLUSIONS

Existing methods have been unable to provide any direct evidence for stress transmission mechanisms between the apical and the basal surface. The AFM-TIRFM system described here allows observation of stress transmission from the apical surface to the basal surface of an adherent cell. Results of this study show that the cell responds globally to the localized applied force over the cell edge and the nucleus. The nuclear region of the cell appears to be stiffer than the rest of the cell body as measured by the AFM. Although the nucleus appears to be offset from the basal surface (TIRFM), the focal adhesion movement upon the apical cell surface perturbation shows that there is a link between the nucleus and the focal adhesions via the cytoskeleton.

This work was supported by National Institute of Health grants HL32132 and HL44972. We also acknowledge the Comprehensive Cancer Center shared Confocal Microscope facility.

REFERENCES

A-Hassan, E., W. F. Heinz, M. D. Antonik, N. P. D'Costa, S. Nageswaran, C.-A. Schoenenberger, and J. H. Hoh. 1998. Relative microelastic mapping of living cells by atomic force microscopy. *Biophys. J.* 74: 1564–1578.

Alberts, B., D. Bray, J. Lewis, M. Raff, K. Roberts, and J. D. Watson. 1994. Molecular Biology of the cell. Garland Publishing, New York.

Axelrod, D., T. P. Burghardt, and N. L. Thompson. 1984. Total internal reflection fluorescence. *Annu. Rev. Biophys. Bioeng.* 13:247–268.

Barbee, K. A., P. F. Davies, and R. Lal. 1994. Shear stress-induced reorganization of the surface topography of living endothelial cells imaged by atomic force microscopy. *Circ. Res.* 74:163–171.

Bausch, A. R., F. Ziemann, A. A. Boulbitch, K. Jacobson, and E. Sackmann. 1998. Local measurements of viscoelastic parameters of adherent cell surfaces by magnetic bead microrheometry. *Biophys. J.* 75: 2038–2049.

Braet, F., C. Rotsch, E. Wisse, and M. Radmacher. 1998. Comparison of fixed and living liver endothelial cells by atomic force microscopy. *Appl. Phys. A.* 66:S575–S578.

Bronkhorst, P. J. H., G. J. Streekstra, J. Grimbergen, E. J. Nijhof, J. J. Sixma, and G. J. Brakenhoff. 1995. A new method to study shape recovery of red blood cells using multiple optical trapping. *Biophys. J.* 69:1666–1673.

Burmeister, J. A., L. A. Olivier, W. M. Reichert, and G. A. Truskey. 1998. Application of total internal reflection fluorescence microscopy to study cell adhesion to biomaterials. *Biomaterials.* 19:307–325.

Burmeister, J. A., G. A. Truskey, and W. M. Reichert. 1994. Quantitative analysis of variable-angle total internal reflection fluorescence microscopy (VA-TIRFM) of cell/substrate contacts. *J. Microsc.* 173:39–51.

Chang, L., T. Kious, M. Yorgancioglu, D. Keller, and J. Pfeiffer. 1993. Cytoskeleton of living, unstained cells imaged by scanning force microscopy. *Biophys. J.* 64:1282–1286.

Christensen, R. M. 1971. Theory of Viscoelasticity: An Introduction. Academic Press, New York.

Davies, P. F. 1995. Flow-mediated endothelial mechanotransduction. *Physiol. Rev.* 75:519–560.

Davies, P. F., A. Robotewskyj, and M. L. Griem. 1993. Quantitative studies of endothelial cell adhesion: directional remodeling of focal adhesion sites in response to flow forces. *J. Clin. Invest.* 93:2031–2038.

Evans, E. A. 1989. Structure and deformation properties of red blood cells: concepts and quantitative methods. *Methods Enzymol.* 173:3–35.

Evans, E. A., K. Ritchie, and R. Merkel. 1995. Sensitive force technique to probe molecular adhesion and structural linkages at biological interfaces. *Biophys. J.* 68:2580–2587.

Evans, E. A., and A. Yeung. 1989. Apparent viscosity and cortical tension of blood granulocytes determined by micropipet aspiration. *Biophys. J.* 56:151–160.

Heidmann, S. R., S. Kaech, R. E. Buxbaum, and A. Matus. 1999. Direct observation of the mechanical behaviors of the cytoskeleton in living fibroblasts. *J. Cell Biol.* 145:109–122.

Henderson, E., and D. S. Sakaguchi. 1993. Imaging f-actin in fixed glial cells with a combined optical fluorescence/atomic force microscope. *Neuroimage.* 1:145–150.

Hochmuth, R. M., J.-Y. Shao, J. Dai, and M. P. Sheetz. 1996. Deformation and flow of membrane into tethers extracted from neuronal growth cones. *Biophys. J.* 70:358–369.

Hofmann, U. G., C. Rotsch, W. J. Parak, and M. Radmacher. 1997. Investigating the cytoskeleton of chicken cardiocytes with the atomic force microscope. *J. Struct. Biol.* 119:84–91.

Ingber, D. E. 1997. Tensegrity: the architectural basis of cellular mechanotransduction. *Annu. Rev. Physiol.* 59:575–599.

Kim, D. W., A. I. Gotlieb, and B. L. Langille. 1989. In vivo modulation of endothelial F-actin microfilaments by experimental alterations in shear stress. *Arteriosclerosis.* 9:439–445.

Maniotis, A. J., C. S. Chen, and D. E. Ingber. 1997. Demonstration of mechanical connections between integrins, cytoskeletal filaments, and

nucleoplasm that stabilize nuclear structure. *Proc. Natl. Acad. Sci. USA.* 94:849–854.

Olivier, L. A., J. Yen, W. M. Reichert, and G. A. Truskey. 1999. Short term cell/substrate contact dynamics of subconfluent endothelial cells following exposure to laminar flow. *Biotechnol. Prog.* 15:33–42.

Radmacher, M. 1997. Measuring the elastic properties of biological samples with the AFM. *IEEE Eng. Med. Biol.* March/April:47–57.

Radmacher, M., M. Fritz, C. M. Kacher, J. P. Cleveland, and P. K. Hansma. 1996. Measuring the viscoelastic properties of human platelets with the atomic force microscope. *Biophys. J.* 70:556–567.

Reichert, W. M., and G. A. Truskey. 1990. Total internal reflection fluorescence (TIRF) microscopy. I. Modelling of cell contact region fluorescence. *J. Cell Sci.* 96:219–230.

Ricci, D., M. Tedesco, and M. Grattarola. 1997. Mechanical and morphological properties of living 3T6 cells probed via scanning force microscopy. *Microsc. Res. Tech.* 36:165–171.

Rotsch, C., F. Braet, E. Wisse, and M. Radmacher. 1997. AFM imaging and elasticity measurements on living rat liver macrophages. *Cell Biol. Int.* 21:685–696.

Rotsch, C., K. Jacobson, and M. Radmacher. 1999. Dimensional and mechanical dynamics of active and stable edges in motile fibroblasts investigated by using atomic force microscopy. *Proc. Natl. Acad. Sci. USA.* 96:921–926.

Sato, M., D. P. Theret, L. T. Wheeler, N. Ohshima, and R. M. Nerem. 1990. Application of the micropipet technique to the measurement of cultured porcine aortic endothelial cell viscoelastic properties. *ASME J. Biomech. Eng.* 112:263–268.

Schoenenberger, C.-A., and J. H. Hoh. 1994. Surface morphology and mechanical properties of MDCK monolayers by atomic force microscopy. *J. Cell Sci.* 107:1105–1114.

Sheetz, M. P., and J. Dai. 1996. Modulation of membrane dynamics and cell motility by membrane tension. *Trends Cell Biol.* 6:85–89.

Simson, D. A., F. Ziemann, M. Strigl, and R. Merkel. 1998. Micropipet-based pico force transducer: in depth analysis and experimental verification. *Biophys. J.* 74:2080–2088.

Stuart, J. K., and V. Hlady. 1999. Reflection interference contrast microscopy combined with scanning force microscopy verifies the nature of protein-ligand interaction force measurements. *Biophys. J.* 76:500–508.

Svoboda, K., C. F. Schmidt, D. Branton, and S. M. Block. 1992. Conformation and elasticity of the isolated red blood cell membrane skeleton. *Biophys. J.* 63:784–793.

Theret, D. P., M. J. Levesque, M. Sato, R. M. Nerem, and L. T. Wheeler. 1988. The application of a homogeneous half-space model in the analysis of endothelial cell micropipette measurements. *J. Biomech. Eng.* 110:190–199.

Wang, N., J. P. Butler, and D. E. Ingber. 1993. Mechanotransduction across the cell surface and through the cytoskeleton. *Science.* 260: 1124–1127.

Wang, N., and D. E. Ingber. 1994. Control of cytoskeletal mechanics by extracellular matrix, cell shape, and mechanical tension. *Biophys. J.* 66:2181–2189.

Wang, N., and D. E. Ingber. 1995. Probing transmembrane mechanical coupling and cytomechanics using magnetic twisting cytometry. *Biochem. Cell Biol.* 73:327–335.

Wechezak, A. R., T. N. Wight, R. F. Viggers, and L. R. Sauvage. 1989. Endothelial adherence under shear stress is dependent upon microfilament reorganization. *J. Cell Physiol.* 139:136–146.

Weisenhorn, A. L., M. Khorsandi, S. Kasas, V. Gotzos, and H.-J. Butt. 1993. Deformation and height anomaly of soft surfaces studied with an AFM. *Nanotechnology.* 4:106–113.

Yamada, K. M., and S. Miyamoto. 1995. Integrin transmembrane signaling and cytoskeletal control. *Curr. Opin. Cell Biol.* 7:681–689.